Hindawi
Geofluids
Volume 2023, Article ID 8861524, 19 pages
https://doi.org/10.1155/2023/8861524

Research Article

Experimental Investigation on Cracking Characteristics of Dry and Saturated Shales in Nitrogen Fracturing after Liquid Nitrogen (LN_2) Injection

Yan Zhang,[1,2,3] **Yu Wu**,[1,2] **Savenok Olga Vadimovna**,[3] **Jiadi Yin**,[1,2] **Haozhe Geng**,[2] **and Decheng Li**[2]

[1]*State Key Laboratory for Geomechanics and Deep Underground Engineering, China University of Mining and Technology, Xuzhou, Jiangsu 221116, China*
[2]*School of Mechanics and Civil Engineering, China University of Mining and Technology, Xuzhou, Jiangsu 221116, China*
[3]*Faculty of Oil and Gas, Saint Petersburg Mining University, Saint Petersburg 199106, Russia*

Correspondence should be addressed to Yu Wu; wuyu@cumt.edu.cn

Received 16 December 2022; Revised 27 February 2023; Accepted 4 March 2023; Published 13 April 2023

Academic Editor: Yi Xue

Cryogenic LN_2 fracturing is one of the environmentally friendly waterless fracturing technologies that promote the fracture complexity of shale gas reservoir. The water-ice phase transition under freezing condition causes frost heave in saturated shale. The effect of moisture in shale should be taken into account during cryogenic damage process. Therefore, the differences of cracking characteristics between dry and saturated shales were studied in this paper. A laboratory triaxial and high temperature fracturing system was developed for nitrogen fracturing dry and saturated shale after LN_2 injection. The influence of moisture on breakdown pressure was studied under different confining pressures (3 MPa, 6 MPa, 9 MPa, and 12 MPa) and bedding directions (parallel bedding and vertical bedding). The experimental results demonstrated that when the confining pressure increased from 3 MPa to 12 MPa, the breakdown pressure of dry parallel bedding after LN_2 preconditioning decreased 7.12 MPa, 6.06 MPa, 4.58 MPa, and 3.11 MPa, respectively. Therefore, LN_2 preconditioning could damage shale resulting in a lower breakdown pressure, but the effect of cryogenic damage decreased with the confining pressure increasing. The moisture in shale had little impact on nitrogen fracturing without LN_2 injection because the breakdown pressure difference between dry and saturated shales was small. However, the breakdown pressure of saturated shale after LN_2 preconditioning was always lower than that of dry shale. The breakdown pressure of saturated parallel bedding shale after LN_2 injection decreased 8.62 MPa, 7.67 MPa, 6.08 MPa, and 4.63 MPa, respectively, with the confining pressure increasing from 3 MPa to 12 MPa. The breakdown pressure difference between dry and saturated shales was impacted by the migration of unfrozen water and frost heave. In addition, the extent of cryogenic damage varied substantially between different bedding directions. When the confining pressure was 3 MPa, the breakdown pressure of saturated parallel bedding shale reduced by 69.18% after LN_2 preconditioning, but that of saturated vertical bedding shale only decreased by 22.49%. The tensile strength of shale had a greater influence on the breakdown pressure. According to the Brazilian disc test results, the tensile strength of matrix was much higher than that of bedding planes. As a result, it is useful to wet the shale in order to reduce the breakdown pressure. The fracturing direction of horizontal drilling should be consistent with the bedding direction for better cryogenic fracturing effect.

1. Introduction

Shale gas is plentiful and extensively spread throughout China, which exceeds 2.2×10^{13} m^3 [1]. The production of shale gas increased rapidly from 2×10^8 m^3 in 2013 to 1.5×10^{10} m^3 in 2019 [2]. The exploitation of shale gas reservoirs has always been restricted by the ultralow permeability, significant in situ horizontal stress differential, enormous burial depth, and low brittleness index [3]. Hydraulic fracturing has been used to stimulate the unconventional gas

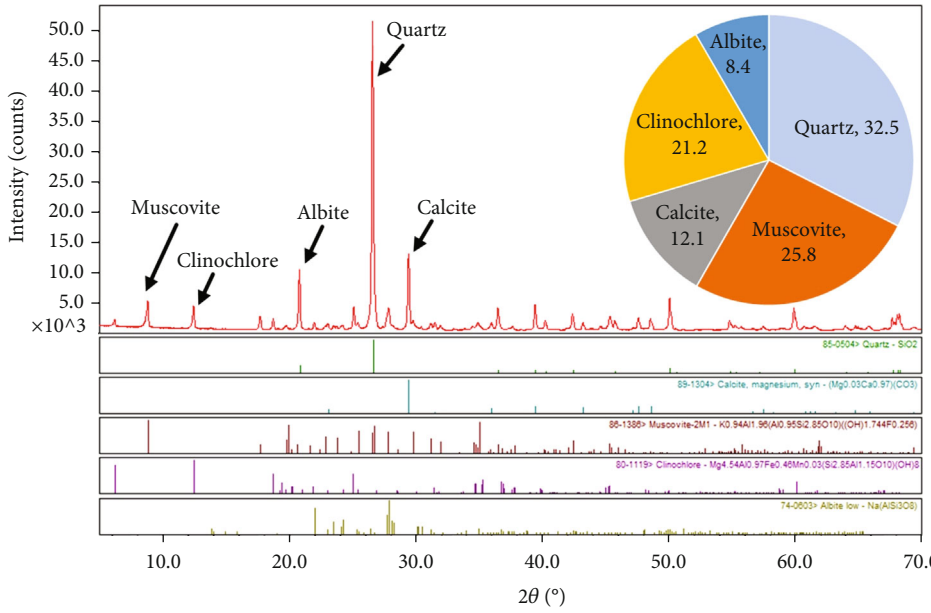

Figure 1: Mineralogy analysis of shale sample.

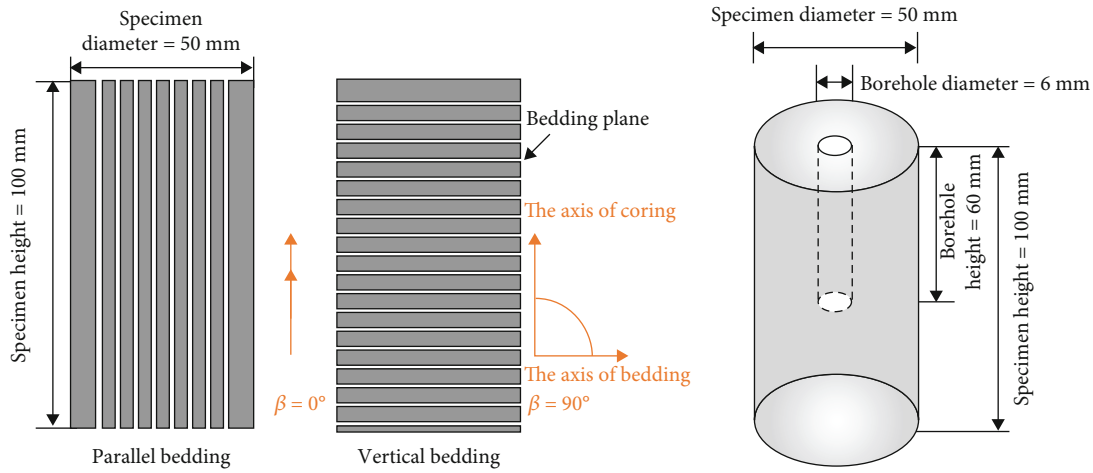

Figure 2: Sample preparation.

reservoir for enhancing the complexity of fracture system [4, 5]. The merits of hydraulic fracturing technology include its low cost and convenient availability [6]. However, the shortcomings are obvious in the process of fracturing. First, shale gas reservoir contains clay minerals. These minerals are prone to swelling, resulting in water lock. Meanwhile, the mineral hydration takes place, resulting in a reduction of effective permeability [7]. Second, water-based fracturing fluids contain chemical impurities and toxic compositions. These synthetics inevitably linger in gas reservoirs and threaten clean water resources [8]. Moreover, the purification treatments increase the development cost. Third, water usage for hydraulic fracturing ranges from 1400 m^3 to 33900 m^3 per horizontal well [9, 10]. The shale gas reservoirs are located in hilly and arid regions, such as Wuning area and Sichuan Basin in China [11]. Therefore, novel waterless fracturing fluids have been drawn attention to solve the water-related issues.

There have been many studies on waterless fracturing fluids, such as liquefied petroleum gases [12–14], supercritical carbon dioxide or liquid carbon dioxide [15–17], high energy gas [18, 19], nitrogen foam [20, 21], and LN_2 [6, 11]. These waterless fracturing technologies have been applied. The burial depth of recoverable shale gas reservoirs ranges between 1000 m and 5000 m. The shale reservoir temperature is high [22]. LN_2 fracturing technology has received more concentration among waterless fracturing technologies. For example, the reservoir temperature of Cooper Basin reaches 150°C at the burial depth of 3500 m [23]. When LN_2 is delivered to the shale gas reservoir, a sharp thermal gradient of more than 300°C is generated in the local area of shale formation. The high local thermal stress induces primary

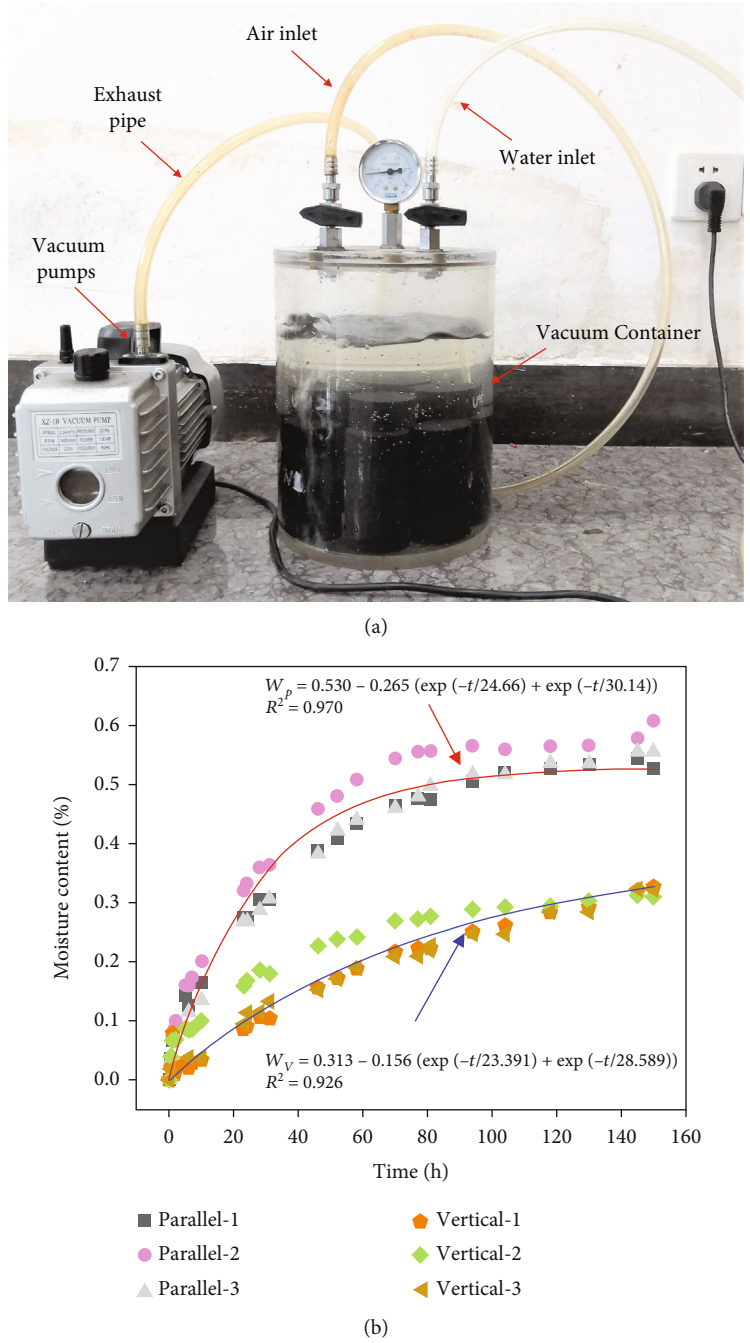

Figure 3: (a) Vacuum-saturated device. (b) Moisture content-time curve of shale sample.

fractures and promotes secondary development of preexisting fractures [24]. Laboratory studies demonstrated that the injection pressure decreased 40% under LN_2 fracturing [25, 26]. The shortage of LN_2 fracturing is the high equipment cost. The drilling pipelines and fracturing pumps bear the burden of adapting the high pressure and low viscosity characteristics of LN_2 [27]. A novel fracturing technology proposed that LN_2 was utilized as assist-gas fluid to cryogenic damage of the reservoir, and nitrogen was used as fracturing fluid to improve the fracture complexity [28]. Both LN_2 and nitrogen are easy to flowback and friendly towards the environment [29, 30].

The effect of cryogenic damage after LN_2 preconditioning is affected by not only the environmental factors such as reservoir temperature, ground stress, and moisture content but also the internal structure factors such as mineralogical composition, microcracks, and bedding orientation [31, 32]. The cryogenic damage extent of frost heave is controlled by initial moisture content [33]. When water freezes, its volume expands by 9%. Besides, the unfrozen water is repelled by disjoining force and moves to the growing ice. More microcracks develop under the freezing condition [34]. Numerous studies have investigated the mechanisms of frost heave and established models to explain the microcrack

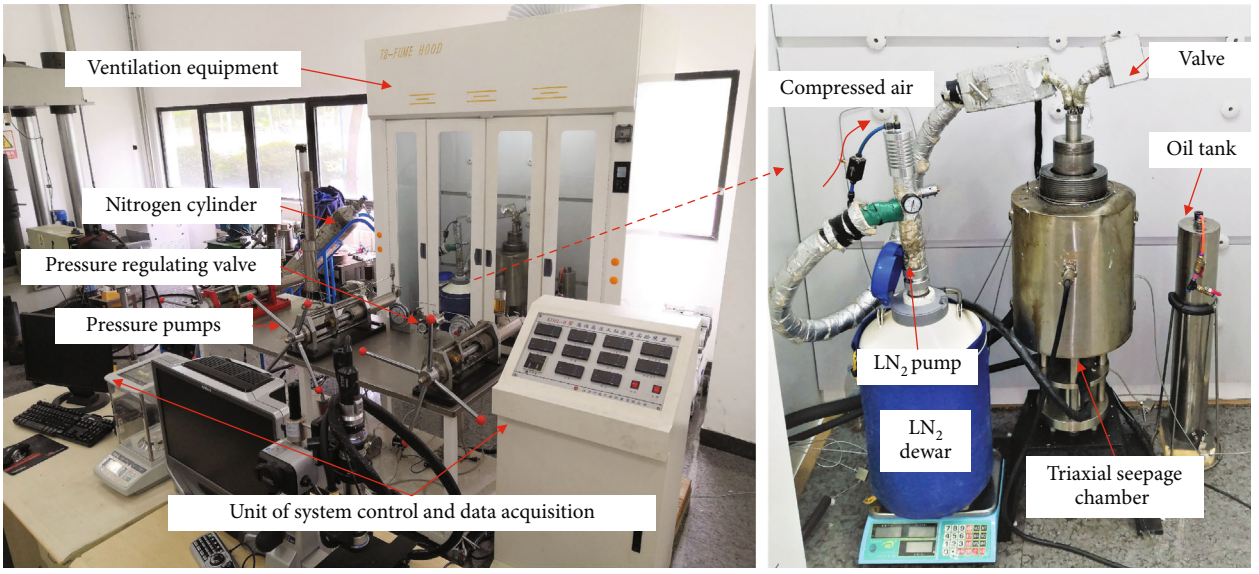

(a)

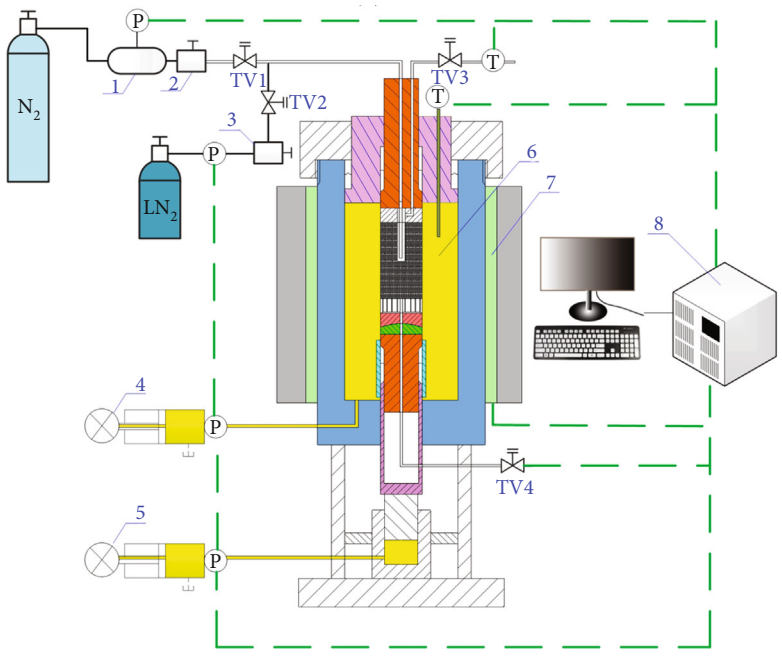

1 High pressure gasholder
2 Nitrogen pressure regulating valve
3 LN_2 pressure regulating valve
4 Confining pressure pump
TV1 Nitrogen inlet valve
TV2 LN_2 inlet valve
Ⓟ Pressure sensor
5 Axial pressure pump
6 Triaxial pressure chamber
7 Electric heating device
8 Real-time data collection system
TV3 LN_2 outlet valve
TV4 Nitrogen outlet valve
Ⓣ Temperature sensor

(b)

Figure 4: (a) The experimental device. (b) Diagram of real triaxial seepage and fracturing device.

generation and the process of ice crystallization [35–37]. However, the studies on the cryogenic damage of low-permeability rocks by frost heave need to be further improved. For example, the breakdown pressure variation of saturated shale after LN_2 preconditioning is neglected because of the low moisture content.

In this paper, the cracking characteristics of dry and saturated shales after LN_2 preconditioning were studied by

Table 1: Experimental scheme.

Experimental group	Influence factors			
	Bedding direction	Moisture content	LN_2 preconditioning time (min)	Confining pressure (MPa)
1	Parallel	Saturated	0	3, 6, 9, 12
2			15	
3		Dry	0	
4			15	
5	Vertical	Saturated	0, 15	3
6		Dry		

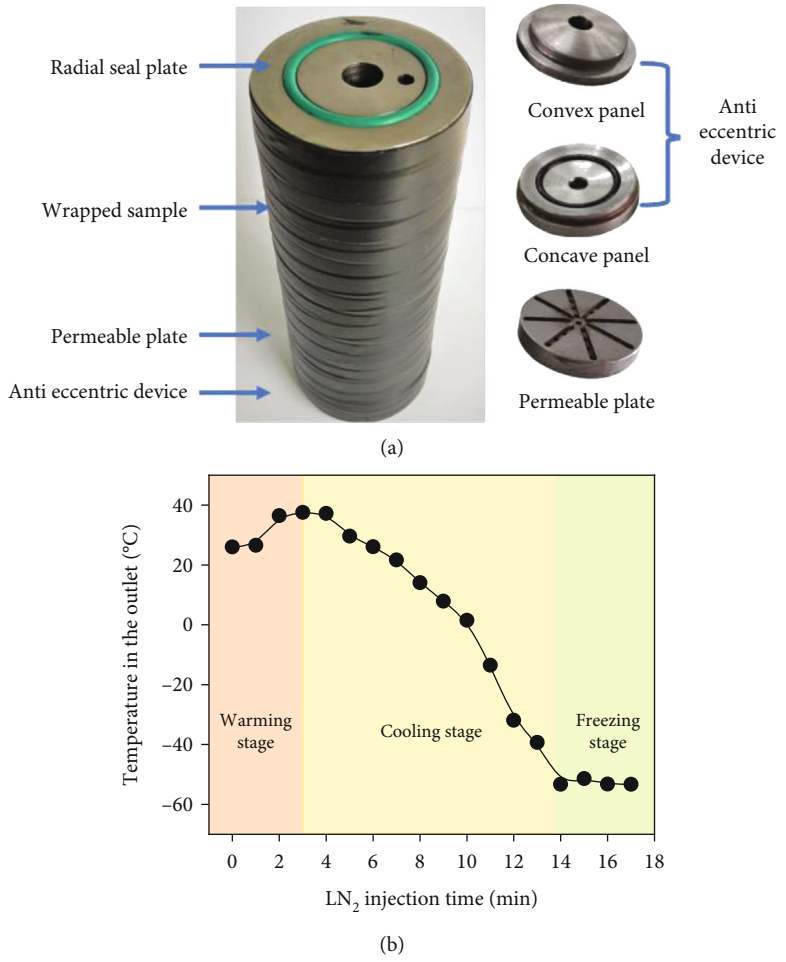

Figure 5: (a) The assembly of sample in the triaxial device. (b) The change of LN_2 outlet temperature.

performing lots of laboratory experiments. First, X-ray diffractometer (XRD) was assisted in the mineralogy analysis on the shale. Second, a laboratory triaxial and high-temperature fracturing system was developed. The nitrogen fracturing after LN_2 preconditioning tests was performed at confining pressure (3 MPa, 6 MPa, 9 MPa, and 12 MPa) and high temperature (100°C) to investigate the breakdown pressure characteristics between dry and saturated shales. Thirdly, the fracture surface of shale was observed by optical microscope to study its macroscopic damage fracture characteristics. Finally, the tensile strength was tested to explain the breakdown pressure difference between different bedding directions. The experimental investigation evaluates the cryogenic damage effect between dry and saturated shales after LN_2 preconditioning. The analysis of frost heave provides insight into cryogenic LN_2 fracturing technology.

2. Experimental Preparation and Methods

2.1. Materials. The shale blocks were collected from the Wuning area, Jiangxi Province, China. It belongs to the Upper Ordovician Xinkailing Formation [38–40]. An X-ray diffractometer (XRD) was used to investigate the mineral composition of shale. The result is plotted in Figure 1. The

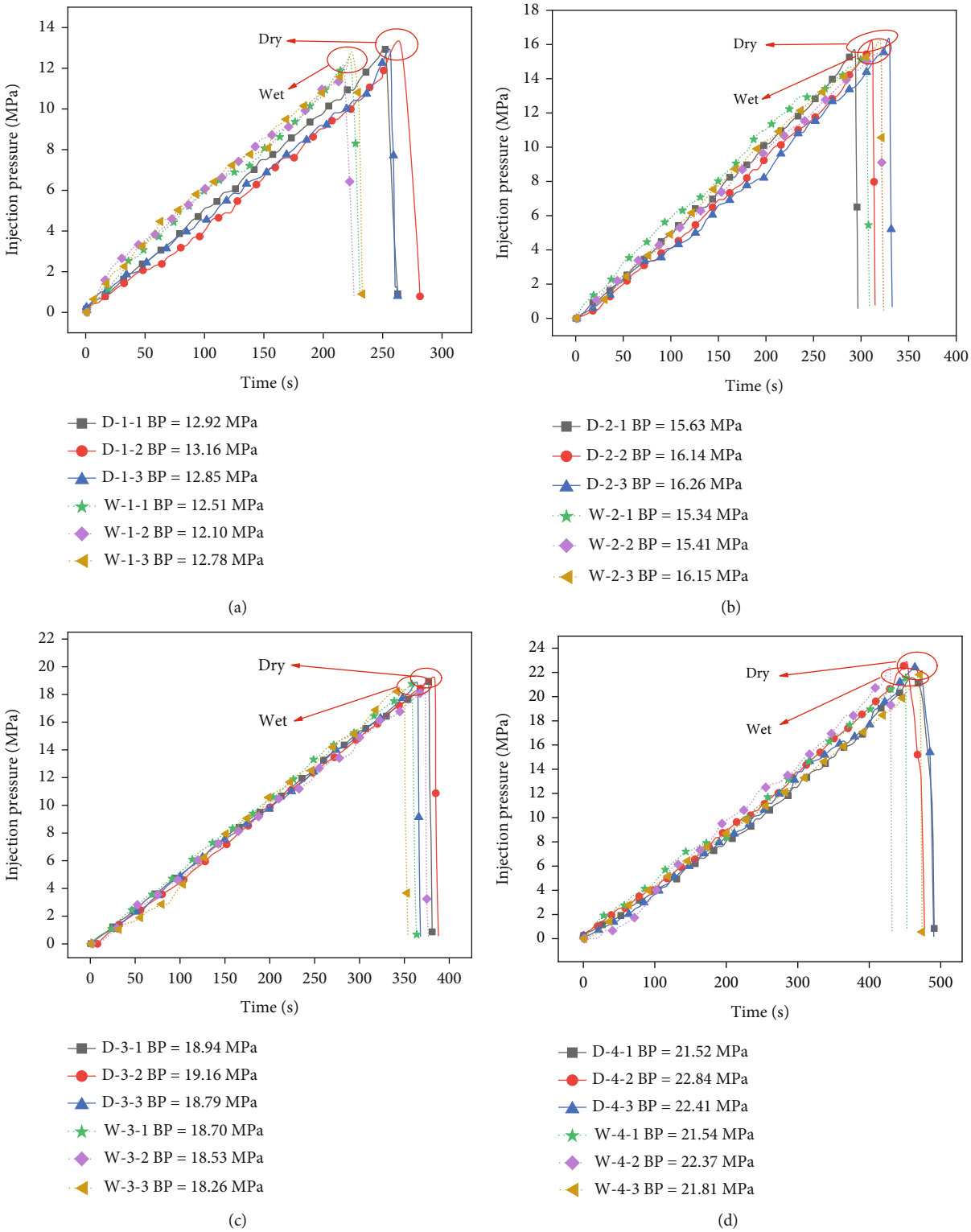

Figure 6: The nitrogen fracturing curves of dry and saturated parallel bedding shales without LN_2 injection under different confining pressures: (a) confining pressure = 3 MPa; (b) confining pressure = 6 MPa; (c) confining pressure = 9 MPa; (d) confining pressure = 12 MPa.

primary constituents of shale were quartz, clinochlore, calcite, muscovite, and albite. The siliceous minerals of shale sample include quartz and albite, accounting for 40.9% of the main components. These minerals offer the benefits for the formation of organic-rich shale [41]. High siliceous content is also favorable for fracturing shale reservoir [42–44]. Inorganic micropores in shale are readily preserved in the process of deposition and conducive to hydrocarbon storage [45]. The formation of inorganic micropores is related to clay minerals [46]. The clay mineral of shale sample was

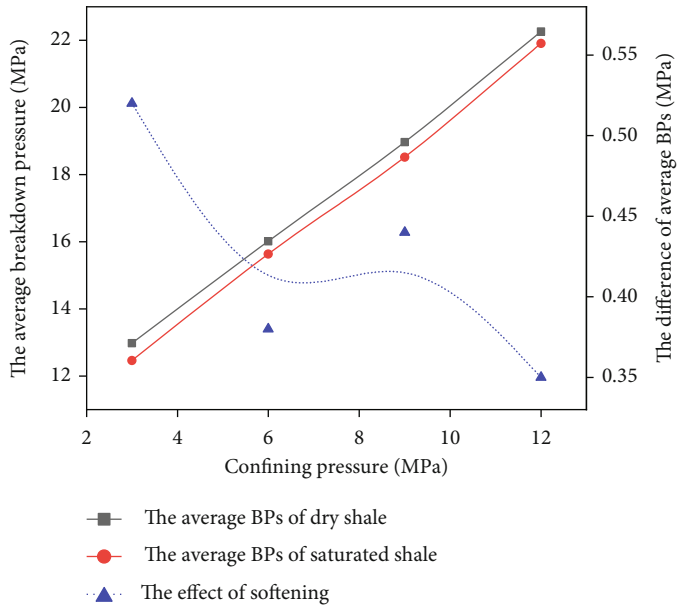

FIGURE 7: The breakdown pressure variation and the difference of average breakdown pressure between dry and saturated shales without LN_2 preconditioning under different confining pressures.

clinochlore, accounting for 21.2% of the main components. Therefore, the Upper Ordovician Xinkailing Formation shale has development potential.

2.2. Shale Sample Preparation. Shale is one of the sedimentary rocks with many alternating beddings of thin and thick layers. These beddings greatly affect the mechanical properties of shale. Therefore, two bedding angles ($\beta = 0\circ, 90^\circ$, as shown in Figure 2) were selected in the experiments. The shale block was cored as cylinders following the ASTM standard [47, 48]. A borehole was drilled for LN_2 preconditioning and nitrogen fracturing in triaxial high-temperature system. The diameter of borehole was 6 mm and the length was 60 mm.

The cylinders were heated in a 110°C oven until the weight no longer changed. The dry shale mass was m_d. Then, the dry samples were placed into a vacuum container. The vacuum saturation method was used to prepare saturated samples. The pressure of the container was maintained at -0.1 MPa for one hour. Air was expelled from the shale pores under negative pressure. Then, open the water inlet until the dry samples were submerged, as shown in Figure 3(a). The negative pressure was maintained during the process of water injection. The wet sample was weighed every two hours and recorded as m_s. The moisture content (ω) can be simply estimated by Equation (1). The wet sample was saturated when the moisture content no longer increased. The moisture content variation is illustrated in Figure 3(b). There were two curves of moisture content between different bedding directions. The mean moisture content of the saturated samples with parallel bedding was 0.530%, while that with vertical bedding was only 0.313%. The average shale mass of dry vertical bedding shale samples was 528.91 g, but that of dry parallel bedding shale was 520.48 g. The shale sample with vertical bedding was denser with fewer micropores and microcracks.

$$\omega = \frac{m_s - m_d}{m_d} \times 100\%. \quad (1)$$

2.3. Experimental Methods. An experimental device was designed for nitrogen fracturing shale in the in situ condition as shown in Figure 4(a). The device is capable of heating sample to 300°C and exerting triaxial pressure (up to 60 MPa). There are four experimental units in the device: a LN_2 injection unit, a high-temperature and triaxial pressure unit, a nitrogen fracturing unit, and a real-time data collection unit as shown in Figure 4(b). The detailed introduction of experimental device was published on another articles [28, 49, 50].

The axial pressure was kept at 30 MPa to prevent gas leakage during the injection of LN_2 and nitrogen fracturing. The sample temperature was set to 100°C for simulating the in situ temperature. The experimental variables are listed in Table 1. The cracking characteristics of dry and saturated shales after LN_2 injection were investigated by the six experimental groups under different confining pressures and bedding orientations.

2.4. Experimental Procedure. The experiment was mainly divided into two stages: the cryogenic damage stage by LN_2 injection and the fracturing stage by nitrogen injection. The injection of LN_2 was as follows:

(1) The assembly sample was installed into the triaxial pressure chamber. The radical seal plate, shale sample with borehole, permeable plate, and antieccentric

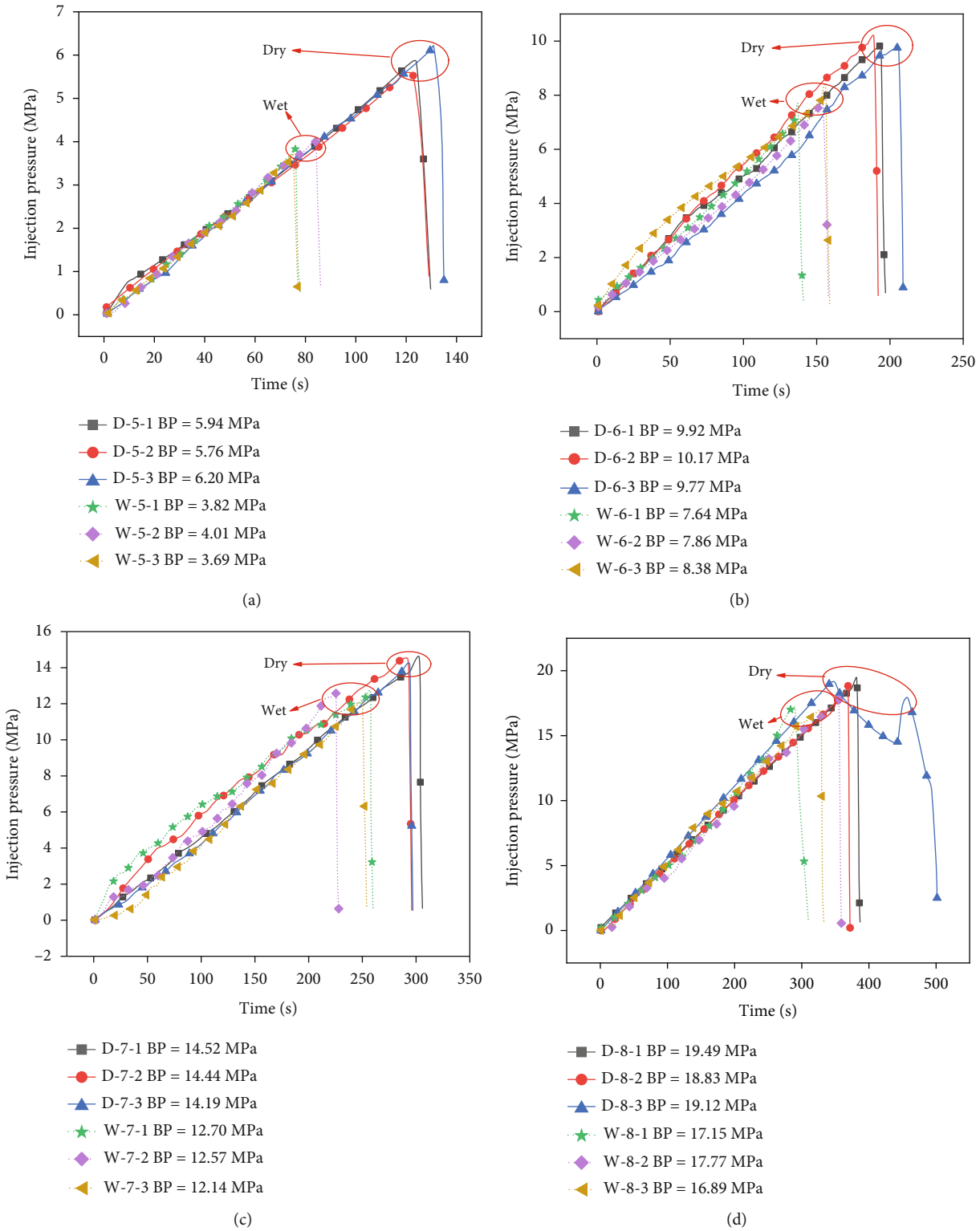

Figure 8: The nitrogen fracturing curves of dry and saturated parallel bedding shales after LN_2 injection under different confining pressures: (a) confining pressure = 3 MPa; (b) confining pressure = 6 MPa; (c) confining pressure = 9 MPa; (d) confining pressure = 12 MPa.

device were assembled together, as shown in Figure 5(a)

(2) The experimental axial pressure was applied to 30 MPa using the pressure pump. The confining pressure was adjusted to the target values (3, 6, 9, and 12 MPa) according to the experimental scheme. The temperature of heating device was maintained at 100°C for 2 h before the injection of LN_2. As a result, the shale sample could be heated to 100°C

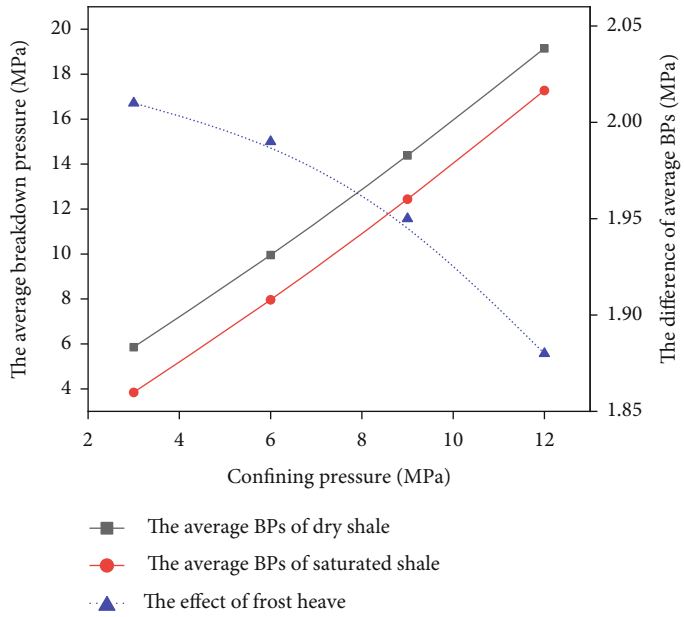

Figure 9: The average breakdown pressure variation and difference between dry and saturated shales after LN_2 preconditioning under different confining pressures.

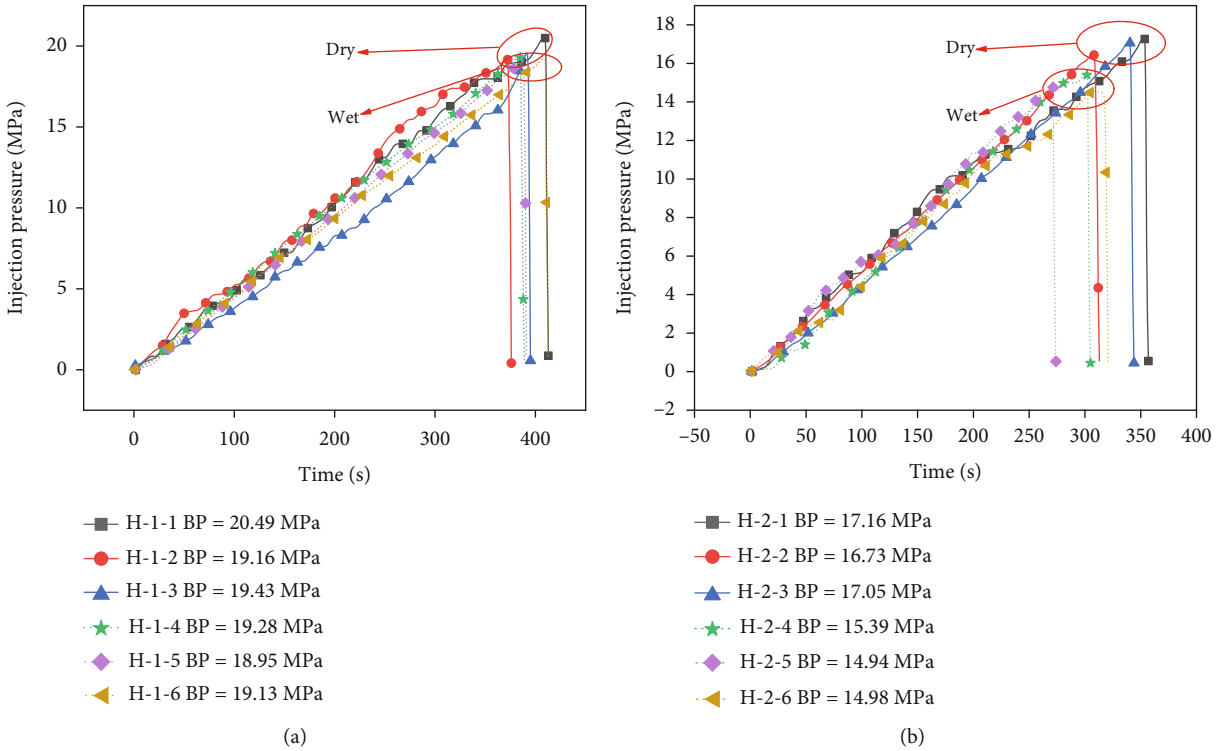

Figure 10: The nitrogen fracturing curves of dry and saturated vertical bedding shales under 3 MPa confining pressures with and without LN_2 injection: (a) without LN_2 injection; (b) with LN_2 injection.

(3) Before LN_2 preconditioning, the nitrogen valves (TV1 and TV4) were closed, and the LN_2 valves (TV2 and TV3) were turned on to facilitate the injection of LN_2 into the specimen for cryogenic damage

(4) LN_2 was delivered into the borehole of shale sample by the LN_2 pump. The injecting rate was controlled at 0.2 L/min. The residual LN_2 was discharged from the LN_2 outlet valve (TV3)

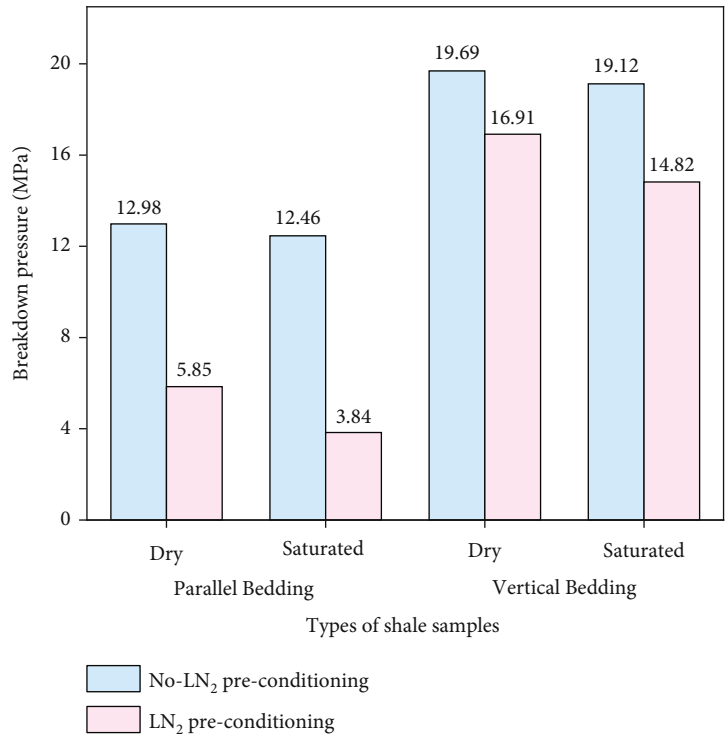

Figure 11: Average breakdown pressure comparison between parallel and vertical bedding shales.

(5) The process of LN_2 preconditioning lasted 15 min. The injection pressure and outlet temperature were monitored by computer

The temperature variation of the LN_2 outlet (TV3) is illustrated in Figure 5(b). There were three stages in the process of LN_2 preconditioning. The outlet temperature increased from 26.0°C to 37.6°C in the warming stage. LN_2 was completely vaporized and extracted heat from the shale surface. The temperature of outlet decreased from 37.6°C to -53.3°C during the cooling stage. The rate of the shale temperature reduction was greater than the thermal compensation rate of heating device. The outlet temperature remained steady at -53.3°C in the freezing stage. A water-ice phase transition occurred, resulting in frost heave.

The procedures of nitrogen fracturing were as follows:

(1) The nitrogen inlet and outlet valves (TV1 and TV4) were turned on to facilitate the injection of nitrogen into the specimen borehole, while the LN_2 inlet and outlet valves (TV2 and TV3) were turned off

(2) The nitrogen pressure regulating valve was used to inject nitrogen into the shale borehole. The rate of pressurization was 50 kPa/s. The variation of injection pressure was monitored by pressure sensor. When the nitrogen flowed out of the nitrogen outlet valve (TV4), the shale specimen was split into halves. The peak pressure was the breakdown pressure of shale

3. Experimental Results

3.1. The Breakdown Pressure Characteristics of Dry and Saturated Shales before LN_2 Preconditioning. Comparing the experimental results between group 1 and group 3, the nitrogen fracturing curves for dry and saturated parallel bedding shales without LN_2 preconditioning are plotted in Figures 6(a)–6(d). The increase of injection pressure was approximately linear by pressure regulating valve during nitrogen fracturing. The end signal of nitrogen fracturing was a sharp reduction of injection pressure. Therefore, the peak of injection pressure was the breakdown pressure (BP) of shale.

When the confining pressure increased from 3 MPa to 12 MPa, the average breakdown pressures of dry samples were 12.98 MPa, 16.01 MPa, 18.96 MPa, and 22.26 MPa, respectively, and those of saturated samples were 12.46 MPa, 15.63 MPa, 18.52 MPa, and 21.91 MPa, respectively. The breakdown pressure variation and the average breakdown pressure differences between dry and saturated shales are plotted in Figure 7. The increase in average breakdown pressure was approximately linear in relation to the increase in confining pressure. In addition, there was little variation between dry and saturated shale samples without LN_2 preconditioning. The differences of average breakdown pressures were 0.51 MPa, 0.38 MPa, 0.44 MPa, and 0.35 MPa with the confining pressure increasing. Therefore, the softening influence decreased with the confining pressure increasing, and the effect of softening was small on the breakdown pressure without LN_2 injection.

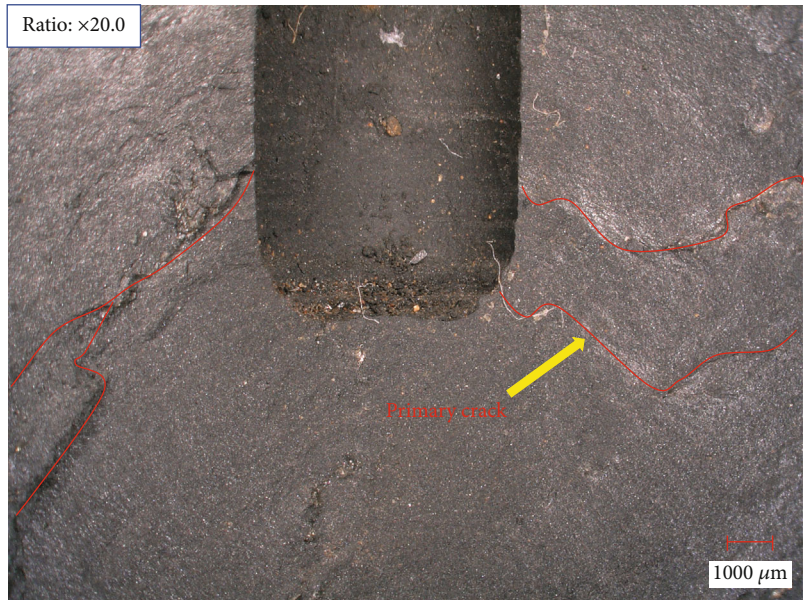

(a)

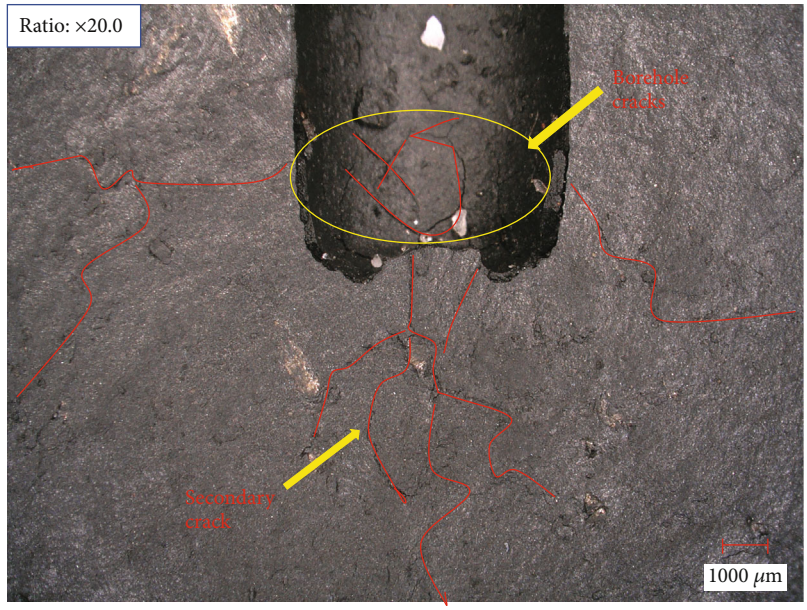

(b)

Figure 12: Continued.

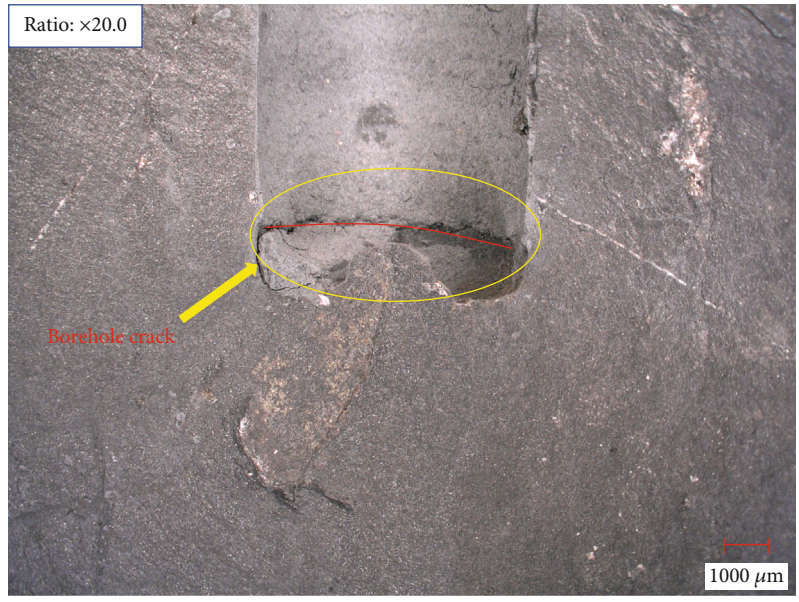

(c)

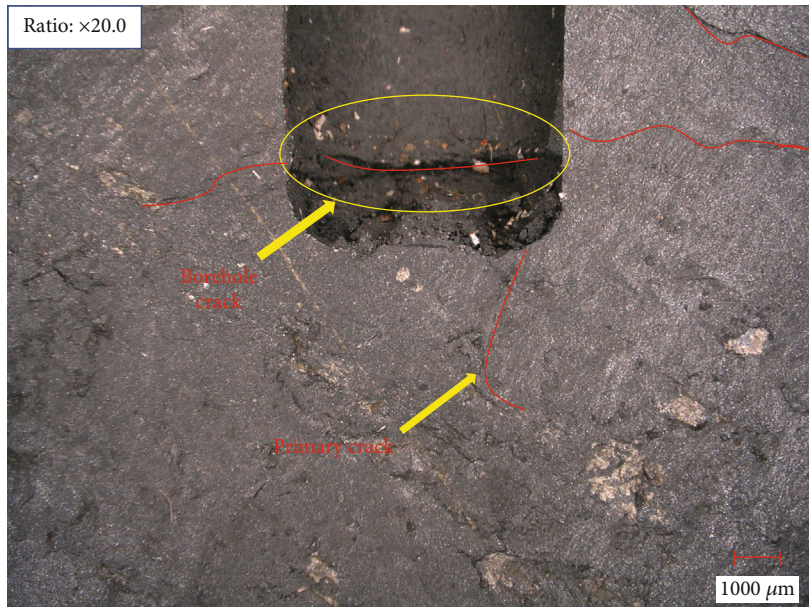

(d)

Figure 12: The crack propagation around the borehole: (a) dry and parallel bedding shales; (b) saturated and parallel bedding shales; (c) dry and vertical bedding shales; (d) saturated and vertical bedding shales.

3.2. The Breakdown Pressure Characteristics of Dry and Saturated Shales after LN_2 Preconditioning. The nitrogen fracturing curves of dry and saturated parallel bedding shales after LN_2 injection are plotted in Figures 8(a)–8(d), when the experimental results between group 2 and group 4 were compared. Most curves of injection pressure were approximately linear by pressure regulating valve during nitrogen fracturing, but there was one special sample that underwent two fracturing processes. When the confining pressure was 12 MPa, the D-8-3 sample was not completely split into two halves at the first peak pressure. The injected nitrogen remained in the shale borehole and could not be exhausted through the nitrogen outlet. The nitrogen continued to be injected into the D-8-3 sample by the nitrogen pressure regulating valve until the sample was finally fractured. The second peak pressure was lower than the first peak pressure. The fracture closed rapidly under the high confining pressure during the first fracturing stage. Therefore, the high confining pressure was not conductive to the propagation of macrocracks.

The average breakdown pressures of dry shale with LN_2 preconditioning were 5.85 MPa, 9.92 MPa, 14.38 MPa, and 19.14 MPa, respectively, and those of saturated shale were 3.84 MPa, 7.96 MPa, 12.44 MPa, and 17.27 MPa as the

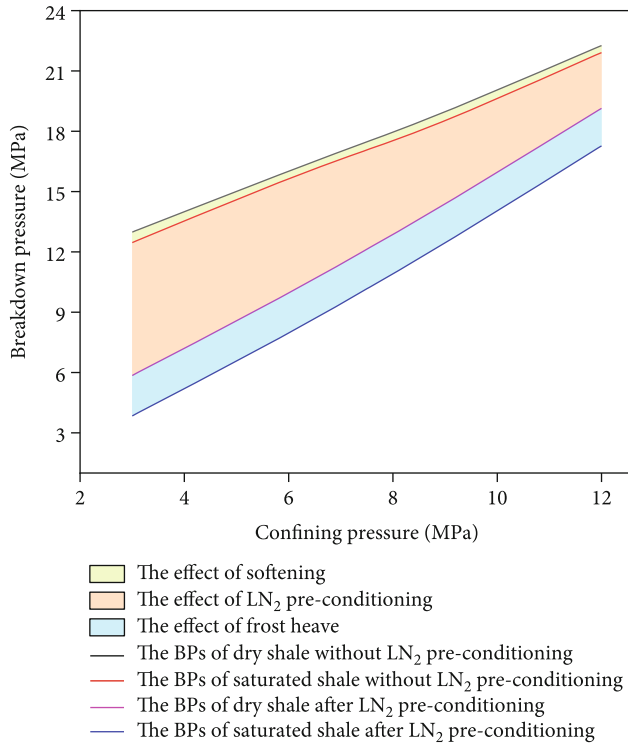

Figure 13: Average breakdown pressure of dry and saturated parallel bedding shales under different confining pressures.

confining pressure grew. Therefore, the cryogenic damage effect was significant by LN_2 injection. The breakdown pressure of dry and saturated shales both decreased after LN_2 injection compared to the experimental results of group 1 and group 3.

After LN_2 preconditioning, the curves of average breakdown pressure differences between dry and saturated shales are plotted in Figure 9. The average breakdown pressures of saturated shale decreased 2.01 MPa, 1.99 MPa, 1.94 MPa, and 1.88 MPa, respectively, compared to those of dry shale. The water-ice phase transition under freezing condition causes frost heave in saturated shale. The effect of frost heave was at least 3.9 times more than that of softening. When the confining pressure increased, the average breakdown pressure difference after LN_2 injection still decreased.

3.3. The Breakdown Pressure Characteristics of Dry and Saturated Shales between Different Bedding Directions after LN_2 Preconditioning. The nitrogen fracturing curves of dry and saturated vertical bedding shales are plotted in Figures 10(a) and 10(b). The average breakdown pressure of dry vertical bedding shale without LN_2 preconditioning was 19.69 MPa, and that of saturated vertical shale was 19.12 MPa. There was only 0.57 MPa reduction under the moisture content. After LN_2 preconditioning, the average breakdown pressure decreased by 14.12% and 22.49% between dry and saturated shales. The difference of average breakdown pressure between dry and saturated vertical bedding shales was 2.09 MPa after LN_2 preconditioning. Therefore, the moisture in shale promoted the effect of LN_2 preconditioning.

The average breakdown pressures between parallel and vertical bedding shales at the confining pressure of 3 MPa are shown in Figure 11. The bedding direction had a great influence on the nitrogen fracturing. The average breakdown pressures of vertical bedding shale were all higher than those of parallel bedding shale. Moreover, the average breakdown pressure difference between parallel bedding and vertical bedding shales increased after LN_2 preconditioning.

New microcracks of shale were formed during the process of LN_2 preconditioning, and the cracks spread by nitrogen injection. The propagation of cracks around the borehole after LN_2 preconditioning is illustrated in Figures 12(a)–12(d). The number of cracks on saturated fracture surface was more than that on dry fracture surface. There were only a few single primary cracks around the dry borehole. However, many secondary cracks were generated around the saturated borehole, forming a complex fracture network. The number of cracks on parallel bedding fracture surface was more than that of vertical bedding fracture surface. Therefore, saturated parallel bedding shale was easy to fracture after LN_2 preconditioning. In addition, the cracks preferred to propagate along the bedding direction.

4. Discussions

According to the observations of the nitrogen fracturing dry and saturated parallel bedding shales after LN_2 preconditioning, the curves of breakdown pressure under different confining pressures are depicted in Figure 13. The breakdown pressure difference between dry and saturated shales

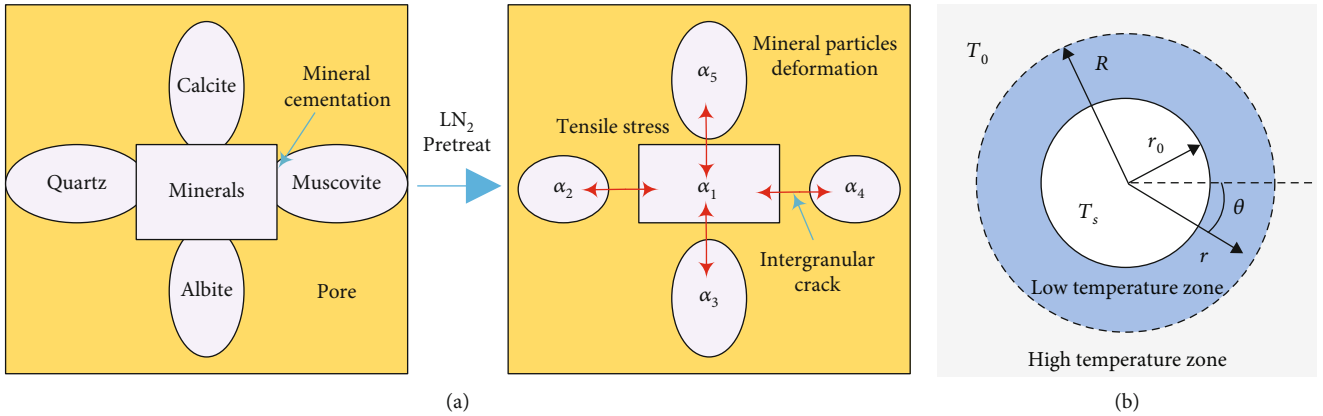

Figure 14: (a) Diagram of mineral particle shrinkage after LN_2 preconditioning. (b) Diagram of temperature field around the borehole during LN_2 preconditioning.

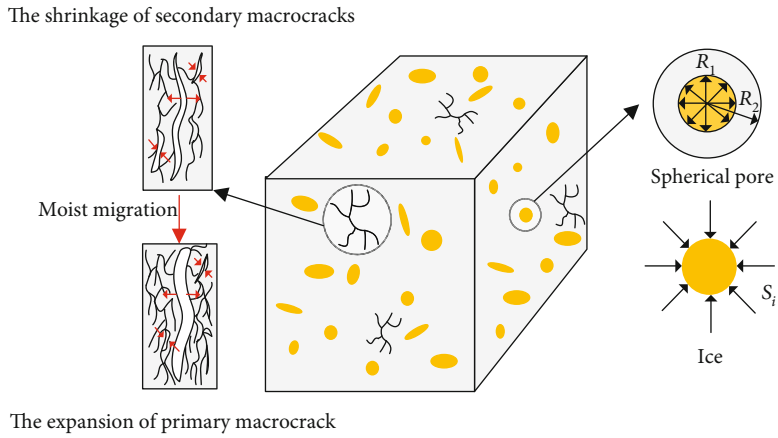

Figure 15: The propagation of spherical pore and primary macrocracks under frost heaving.

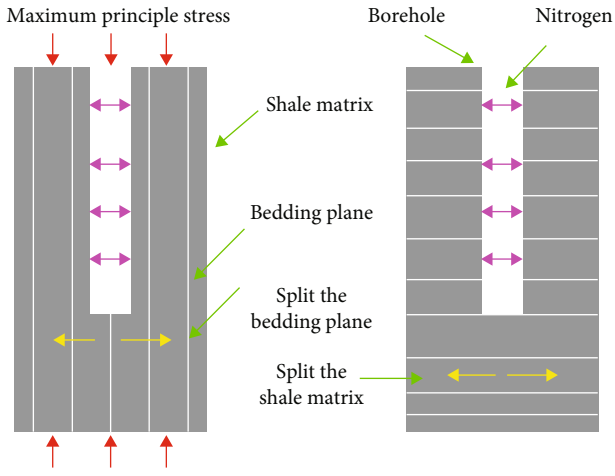

Figure 16: Diagram of shale in the nitrogen fracturing test.

without LN_2 preconditioning was small. There were muscovite and clay minerals in shale. The hydration and expansion stress lead to the fragmentation and disintegration of mineral particles. Although these minerals hydrate with water in pores and macrocracks and expand in volume, there was only 0.53% moisture content in the saturated parallel bedding shale. Therefore, the effect of softening on breakdown pressure was small.

The effect of LN_2 preconditioning was significant, as shown in Figure 13. When LN_2 was delivered to the shale sample at 100°C, a sharp thermal gradient approaching 300°C was generated in the local area. The local thermal stress is the main reason of the cryogenic damage of shale, as shown in Figure 14. There are two types of crack propagation caused by the local thermal stress:

(1) Shale consists of different mineral grains, such as quartz, albite, and muscovite. These mineral particles have different thermophysical and mechanical characteristics. The adjacent mineral particles deform to different degrees during LN_2 preconditioning [51], as shown in Figure 14(a). Intergranular cracks develop as the cementitious strength of minerals is lower than the tensile stress [52]

(2) A violent heat transfer occurs around the borehole, forming a low-temperature zone with LN_2 injection. The zone of low temperature cannot shrink freely

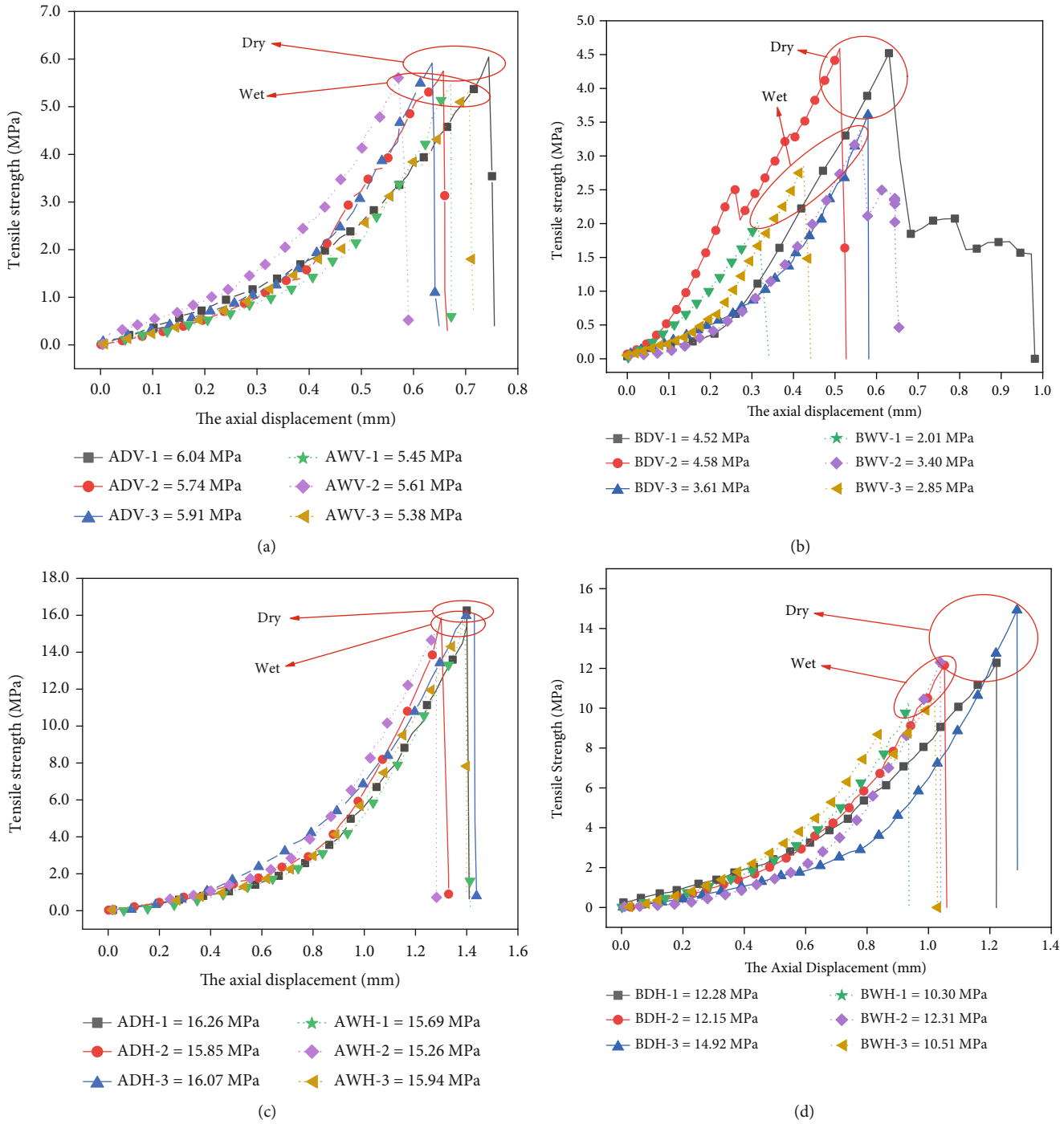

Figure 17: Continued.

(e) (f)

Figure 17: The stress-displacement curve of dry and saturated shales: (a) parallel bedding shales without LN_2 preconditioning; (b) parallel bedding shales after LN_2 preconditioning; (c) vertical bedding shales without LN_2 preconditioning; (d) vertical bedding shales after LN_2 preconditioning. The failure pattern of shale in the Brazilian disc test: (e) parallel bedding shale; (f) vertical bedding shale.

because of the restrictions imposed by the surrounding rock, resulting in the local tensile stress, as shown in Figure 14(b). When the local tensile stress exceeds the shale matrix's tension stress, new cracks form

The damage characteristics of saturated shale samples are more complicated after LN_2 preconditioning, compared to the dry shale samples. When the shale samples were pretreated by LN_2, there was a clear difference between dry and saturated shales, as shown in Figure 13. The water in pores and macrocracks was frozen during LN_2 preconditioning. More cracks were produced due to the frost heave. Furthermore, the effect of frost heave would not decrease with the confining pressure increasing.

There are two mechanical mechanisms of shale fracture driven by ice growth, as shown in Figure 15:

(1) Shale has low permeability; thus, water is hard to flow out the pores in the matrix [53]. If the spherical pores are entirely filled with water as shown in Figure 15, the water will freeze under LN_2 preconditioning. The volume expansion of ice acting on the spherical pore walls causes frost heave. The microcracks develop around the pores when the expansion stress of ice exceeds the tensile stress of pore

(2) Water exists not only in the pores but also in the cracks. There are many interconnected natural cracks. The freezing point of different volume cracks varied due to the capillary effect. The water in the larger crack is more likely to freeze [54]. Therefore, the water in the primary crack freezes under LN_2 preconditioning. When water freezes, its volume expands by 9%. The volume of primary crack keeps growing with the volume expansion of ice. In the frozen fringe, water migrates continuously to ice when the pressure of crack decreases [55]. The water in the secondary cracks migrates to the unfrozen area of primary crack due to the surface-energy effect [56]. Meanwhile, the secondary cracks lose water and shrink during LN_2 preconditioning. The crack deformation is restricted by shale matrix, creating a localized tensile stress. The local tensile stress around the cracks is conductive to the propagation of cracks. Therefore, the migration of water is favorable for the expansion of primary crack

According to the observations of the cracking characteristics between different bedding directions after LN_2 preconditioning, there was wide variation in the average breakdown pressure. As shown in Figure 16, the tensile stress induced by nitrogen injection was applied to the shale borehole. When the injection pressure was greater than the crack initiation pressure, the crack would occur around the shale borehole. The crack propagation tended to spread along the maximum principal stress direction. The axial pressure (30 MPa) was always higher than the confining pressure (3 MPa-12 MPa) during the nitrogen fracturing test. Therefore, the axial direction was the direction of crack. The bedding was one of the discontinuities in shale. When the bedding direction coincided with the direction of fracture propagation, the shale was split along the bedding orientation. The shale matrix was split by the injection pressure while the fracture propagation was vertical to the bedding orientation. Therefore, the reason for the variation of the average breakdown pressure was the different tensile strengths between shale bedding and matrix.

The Brazilian disc tests of dry and saturated shales were conducted to study the different tensile strengths between parallel and vertical bedding directions. The stress-displacement curves of parallel bedding shale are depicted in Figures 17(a) and 17(b). The mean tensile strength of dry parallel bedding shale without LN_2 preconditioning was 5.90 MPa, and that of saturated shale was 5.48 MPa. The difference between dry and saturated shales was small because the moisture in shale had a little influence on the tensile strength. When the parallel bedding shale samples were pretreated by LN_2, the mean tensile strength of dry shale decreased 1.66 MPa and that of saturated shale decreased 2.73 MPa. Therefore, the reduction of tensile strength caused by the frost heave was 1.07 MPa. The frost heave was beneficial for the cryogenic damage. The failure of parallel bedding specimen was a typical splitting mode as shown in Figure 17(e). An approximate linear central fracture was formed along the bedding and split the specimen into halves. Therefore, the tensile strength depended on the bedding cementation.

The stress-displacement curves of vertical bedding shale are depicted in Figures 17(c) and 17(d). Compared to the

tensile strength of parallel bedding shale, that of vertical bedding shale was higher. The mean tensile strength of dry vertical bedding shale without LN_2 preconditioning was 16.06 MPa, which was 2.72 times greater than that of dry parallel bedding shale. The difference of tensile strength between dry and saturated shales was 0.43 MPa. Therefore, the moisture effect on the shale was minimal. After LN_2 preconditioning, the mean tensile strength of dry vertical bedding shale was 13.12 MPa and that of saturated shale was 11.04 MPa. Although the frost heave reduced the tensile strength by 1.65 MPa, the mean tensile strength of vertical bedding shale was still higher than that of parallel bedding shale. The failure of vertical bedding specimen included splitting failure and shear slide modes as shown in Figure 17(f). The propagation of fracture deviated from the loading direction, forming an arc. Moreover, the fractures occurred on the bedding plane, splitting the specimen into slices. Therefore, when the stress loading direction was vertical to the bedding direction, the tensile strength depended on the cementitious force of the matrix, and the bedding direction had an influence on the propagation of fracture. In conclusion, the cementation of bedding was weaker than that of the matrix, and the fracturing direction should be consistent with the bedding direction for relieving the equipment burden and forming more complex fracture network.

5. Conclusions

According to the characteristics of LN_2, we proposed a cryogenic fracturing technology where LN_2 is used as an assisted fluid to cool the shale gas reservoir and nitrogen is used as a fracturing fluid to form more complex crack system. In this paper, the cracking characteristics between dry and saturated shales after LN_2 injection were studied. The subsequent four conclusions are as follows:

(1) The clay minerals offer the benefits for the formation of inorganic nanopores. The inorganic nanopores are readily preserved in the process of deposition and conducive to hydrocarbon storage. The siliceous minerals are also favorable for fracturing shale reservoir. The siliceous minerals and the clay minerals account for 62.1 percent of the main components of shale. Therefore, the Upper Ordovician Xinkailing Formation should be further researched for efficient exploration and exploitation

(2) Although there were muscovite and clay minerals in shale that hydrate with water in pores and macrocracks and expand in volume, the average breakdown pressure difference between dry and saturated shales without LN_2 preconditioning was small. The reason for the phenomenon was the low moisture content of shale. The moisture content of parallel bedding shale was 0.530%, and that of vertical bedding shale was only 0.313%. The average shale mass differential between two bedding directions resulted in varying moisture content. LN_2 preconditioning is beneficial for reducing the breakdown pressure of shale. When the shale surface experiences violent heat transfer, local thermal stress is generated in the temperature gradient direction, causing the crack development. Meanwhile, the breakdown pressure of dry shale with LN_2 preconditioning decreased 7.12 MPa, 6.06 MPa, 4.58 MPa, and 3.11 MPa, respectively, as the surrounding pressure grew. Therefore, the effect of LN_2 preconditioning was constrained by the surrounding pressure

(3) After LN_2 preconditioning, the average breakdown pressures of saturated shale decreased by 69.19%, 50.09%, 32.85%, and 21.17% with the confining pressure increasing from 3 MPa to 12 MPa. The frost heave and migration of unfrozen water are conductive to more microcracks generated and weaken the cementation between bedding planes. Therefore, the LN_2 preconditioning effect of saturated shale is better than that of dry shale. Wetting shale around horizontal drilling before LN_2 preconditioning can facilitate the cryogenic damage effect on the breakdown pressure

(4) The cracking characteristics of vertical bedding shale are influenced by the shale matrix, whereas the bedding plane significantly determines the cracking characteristics of parallel bedding shale. After LN_2 preconditioning, the tensile strength of dry vertical bedding shale was 3.09 times than that of dry parallel bedding shale, and the tensile strength of saturated vertical bedding shale was 4.01 times than that of saturated parallel bedding shale. The frost heave increased the tensile strength difference between dry and saturated shales. The breakdown pressure of vertical bedding shale was also higher than that of parallel bedding shale. Therefore, the fracturing direction of drilling should be parallel to the bedding direction in order to achieve better fracturing effect

Data Availability

The experimental data are available from the corresponding author.

Conflicts of Interest

There are no conflicts to declare.

Acknowledgments

This project was funded by the Postgraduate Research & Practice Innovation Program of Jiangsu Province (grant number KYCX22_2506) and the Assistance Program for Future Outstanding Talents of China University of Mining and Technology (grant number 2022WLKXJ123).

References

[1] Y. Z. Jia, J. R. Tang, Y. Y. Lu, and Z. H. Lu, "Laboratory geomechanical and petrophysical characterization of Longmaxi shale

properties in Lower Silurian formation, China," *Marine and Petroleum Geology*, vol. 124, article 104800, 2021.

[2] C. N. Zou and Z. Qiu, "Preface: new advances in unconventional petroleum sedimentology in China," *Acta Sedimentologica Sinica*, vol. 39, no. 1, pp. 1–9, 2021.

[3] I. Bosikov, R. Klyuev, and A. Mayer, "Comprehensive assessment of hydraulic fracturing technology efficiency for well construction during hydrocarbon production," *Journal of Mining Institute*, vol. 258, pp. 1018–1025, 2022.

[4] M. V. Dvoynikov, D. I. Sidorkin, A. A. Kunshin, and D. A. Kovalev, "Development of hydraulic turbodrills for deep well drilling," *Applied Sciences*, vol. 11, no. 16, p. 7517, 2021.

[5] R. Khuzin, V. Andreev, V. Mukhametshin, L. Kuleshova, G. Dubinskiy, and A. Safiullina, "Influence of hydraulic compression on porosity and permeability properties of reservoirs," *Journal of Mining Institute*, vol. 251, pp. 688–697, 2021.

[6] L. Wang, B. Yao, M. Cha et al., "Waterless fracturing technologies for unconventional reservoirs-opportunities for liquid nitrogen," *Journal of Natural Gas Science and Engineering*, vol. 35, pp. 160–174, 2016.

[7] I. Raupov, R. Burkhanov, A. Lutfullin, A. Maksyutin, A. Lebedev, and E. Safiullina, "Experience in the application of hydrocarbon optical studies in oil field development," *Energies*, vol. 15, no. 10, p. 3626, 2022.

[8] E. Rogov, "Study of the well near-bottomhole zone permeability during treatment by process fluids," *Journal of Mining Institute*, vol. 242, p. 169, 2020.

[9] S. Goodwin, K. Carlson, K. Knox, C. Douglas, and L. Rein, "Water intensity assessment of shale gas resources in the Wattenberg field in northeastern Colorado," *Environmental Science & Technology*, vol. 48, no. 10, pp. 5991–5995, 2014.

[10] B. R. Scanlon, R. C. Reedy, and J. P. Nicot, "Comparison of water use for hydraulic fracturing for unconventional oil and gas versus conventional oil," *Environmental Science & Technology*, vol. 48, no. 20, pp. 12386–12393, 2014.

[11] Z. F. Li, H. F. Xu, and C. Y. Zhang, "Liquid nitrogen gasification fracturing technology for shale gas development," *Journal of Petroleum Science and Engineering*, vol. 138, pp. 253–256, 2016.

[12] J. Z. Zhao, P. F. Chen, Y. Q. Liu, and J. C. Mao, "Development of an LPG fracturing fluid with improved temperature stability," *Journal of Petroleum Science and Engineering*, vol. 162, pp. 548–553, 2018.

[13] P. Chen, H. Chang, G. Xiong, Y. Zhang, and X. Zheng, "Synthesis of phosphates for liquefied petroleum gas (LPG) fracturing fluid," *Applied Petrochemical Research*, vol. 9, no. 3-4, pp. 179–184, 2019.

[14] J. Feng, Q. Sheng, C. W. Luo, and J. Zeng, "The application of hydraulic fracturing in storage projects of liquefied petroleum gas," *Key Engineering Materials*, vol. 306-308, pp. 1509–1514, 2006.

[15] M. H. Ahmadi, S. M. Alizadeh, D. Tananykhin, S. K. Hadi, P. Iliushin, and A. Lekomtsev, "Laboratory evaluation of hybrid chemical enhanced oil recovery methods coupled with carbon dioxide," *Energy Reports*, vol. 7, pp. 960–967, 2021.

[16] R. Syah, S. M. Alizadeh, K. S. Nurgalieva et al., "A laboratory approach to measure enhanced gas recovery from a tight gas reservoir during supercritical carbon dioxide injection," *Sustainability*, vol. 13, no. 21, article 11606, 2021.

[17] Q. Guo, M. H. Ahmadi, M. Lahafdoozian et al., "A laboratory approach on the improvement of oil recovery and carbon dioxide storage capacity improvement by cyclic carbon dioxide injection," *Energy Reports*, vol. 7, pp. 1571–1580, 2021.

[18] J. J. Wu, L. C. Liu, G. H. Zhao, and X. S. Chu, "Research and exploration of high energy gas fracturing stimulation integrated technology in Chinese shale gas reservoir," *Advanced Materials Research*, vol. 524-527, pp. 1532–1536, 2012.

[19] F. P. Wu, X. M. Wei, Z. X. Chen et al., "Numerical simulation and parametric analysis for designing high energy gas fracturing," *Journal of Natural Gas Science and Engineering*, vol. 53, pp. 218–236, 2018.

[20] M. Qu, T. Liang, and J. R. Hou, "Study on fluid behaviors of foam-assisted nitrogen flooding on a three-dimensional visualized fracture–vuggy model," *Applied Sciences*, vol. 11, no. 23, article 11082, 2021.

[21] D. Chen, S. Cui, Z. Liu, Z. Xu, and B. Li, "Study on the stability and rheological properties of nitrogen foam under high-pressure condition," *IOP Conference Series: Earth and Environmental Science*, vol. 632, article 022002, 2021.

[22] W. Guo, H. L. Liu, H. Q. Xue, and X. B. Li, "Research and applications on the theory of shale gas depth enrichment zone," *Advanced Materials Research*, vol. 734-737, pp. 422–425, 2013.

[23] D. Kulikowski, D. Cooke, and K. Amrouch, "Constraining the distribution and relationship between overpressure, natural fracture density and temperature in the Cooper basin, Australia," *The APPEA Journal*, vol. 56, no. 1, pp. 11–28, 2016.

[24] M. Cha, N. B. Alqahtani, B. Yao, X. Yin, and J. L. Miskimins, "Cryogenic fracturing of wellbores under true triaxial-confining stresses: experimental investigation," *SPE Journal*, vol. 23, no. 4, pp. 1271–1289, 2018.

[25] M. Cha, X. Yin, T. Kneafsey et al., "Cryogenic fracturing for reservoir stimulation - laboratory studies," *Journal of Petroleum Science and Engineering*, vol. 124, pp. 436–450, 2014.

[26] N. B. Alqatahni, M. Cha, B. Yao et al., "Experimental investigation of cryogenic fracturing of rock specimens under true triaxial confining stresses," in *SPE Europec featured at 78th EAGE Conference and Exhibitio*, Vienna, Austria, 2016.

[27] S. K. Zhang, Z. W. Huang, H. Y. Zhang et al., "Experimental study of thermal-crack characteristics on hot dry rock impacted by liquid nitrogen jet," *Geothermics*, vol. 76, pp. 253–260, 2018.

[28] Y. Wu, J. Tao, J. H. Wang, Y. Zhang, and S. H. Peng, "Experimental investigation of shale breakdown pressure under liquid nitrogen pre-conditioning before nitrogen fracturing," *International Journal of Mining Science and Technology*, vol. 31, no. 4, pp. 611–620, 2021.

[29] B. Zhao, G. Q. Zhang, P. Y. Zhao, L. L. Wang, Y. Lin, and Y. J. Lv, "Experimental study of mechanics and seepage characteristics of sandstones after liquid-nitrogen stimulation," *Journal of Natural Gas Science and Engineering*, vol. 47, pp. 11–21, 2017.

[30] S. K. Zhang, Z. W. Huang, H. Z. Wang, H. Y. Zhang, C. C. Zhang, and C. Xiong, "Thermal characteristics analysis with local thermal non-equilibrium model during liquid nitrogen jet fracturing for HDR reservoirs," *Applied Thermal Engineering*, vol. 143, pp. 482–492, 2018.

[31] A. Gabova, E. Chekhonin, Y. Popov et al., "Experimental investigation of thermal expansion of organic-rich shales," *International Journal of Rock Mechanics and Mining Sciences*, vol. 132, article 104398, 2020.

[32] B. Liu, Y. D. Sun, J. Wang, and G. Zhang, "Characteristic analysis of crack initiation and crack damage stress of sandstone and mudstone under low-temperature condition," *Journal of Cold Regions Engineering*, vol. 34, no. 3, 2020.

[33] L. Qin, C. Zhai, J. Z. Xu, S. M. Liu, C. Zhong, and G. Q. Yu, "Evolution of the pore structure in coal subjected to freeze –thaw using liquid nitrogen to enhance coalbed methane extraction," *Journal of Petroleum Science and Engineering*, vol. 175, pp. 129–139, 2019.

[34] L. Girard, S. Gruber, S. Weber, and J. Beutel, "Environmental controls of frost cracking revealed through in situ acoustic emission measurements in steep bedrock," *Geophysical Research Letters*, vol. 40, no. 9, pp. 1748–1753, 2013.

[35] J. H. Huang, C. C. Xia, C. L. Han, and S. W. Shen, "Study on the classification and evaluation method of the frost susceptibility of rock mass," *International Symposium on Systematic Approaches to Environmental Sustainability in Transportation*, pp. 28–41, 2015.

[36] T. Sandström, K. Fridh, M. Emborg, and M. Hassanzadeh, "The influence of temperature on water absorption in concrete during freezing," *Nordic Concrete Research*, vol. 45, no. 1, pp. 45–58, 2009.

[37] I. Vlahou and M. G. Worster, "Ice growth in a spherical cavity of a porous medium," *Journal of Glaciology*, vol. 56, no. 196, pp. 271–277, 2010.

[38] S. R. Li, L. Zeng, Z. P. Wang, J. C. Zhang, and D. Ma, "A new insight into shale-gas accumulation conditions and favorable areas of the Xinkailing formation in the Wuning area," *North-West Jiangxi, China, Energies*, vol. 11, no. 1, p. 12, 2017.

[39] G. Wang, Y. Ju, and K. Han, "Early Paleozoic shale properties and gas potential evaluation in Xiuwu basin, western Lower Yangtze platform," *Journal of Natural Gas Science and Engineering*, vol. 22, pp. 489–497, 2015.

[40] K. Zhang, Y. Song, S. Jiang et al., "Shale gas accumulation mechanism in a syncline setting based on multiple geological factors: an example of southern Sichuan and the Xiuwu basin in the Yangtze region," *Fuel*, vol. 241, pp. 468–476, 2019.

[41] L. Wu, D. Hu, Y. Lu, R. Liu, and X. Liu, "Advantageous shale lithofacies of Wufeng formation-Longmaxi formation in Fuling gas field of Sichuan basin, SW China," *Petroleum Exploration and Development*, vol. 43, no. 2, pp. 208–217, 2016.

[42] S. M. Ibad and E. Padmanabhan, "Lithofacies, mineralogy, and pore types in Paleozoic gas shales from Western Peninsular Malaysia," *Journal of Petroleum Science and Engineering*, vol. 212, article 110239, 2022.

[43] X. Wang, R. Wang, W. Ding et al., "Development characteristics and dominant factors of fractures and their significance for shale reservoirs: a case study from $\in_1 b^2$ in the Cen'gong block, southern China," *Journal of Petroleum Science and Engineering*, vol. 159, pp. 988–999, 2017.

[44] L. Wu, Y. Lu, S. Jiang, Y. Lu, X. Liu, and H. Hu, "Pore structure characterization of different lithofacies in marine shale: a case study of the Upper Ordovician Wufeng-Lower Silurian Longmaxi formation in the Sichuan basin, SW China," *Journal of Natural Gas Science and Engineering*, vol. 57, pp. 203–215, 2018.

[45] N. S. Fishman, P. C. Hackley, H. A. Lowers et al., "The nature of porosity in organic-rich mudstones of the Upper Jurassic Kimmeridge clay formation, North Sea, offshore United Kingdom," *International Journal of Coal Geology*, vol. 103, pp. 32–50, 2012.

[46] L. Chen, Z. Jiang, K. Liu et al., "Effect of lithofacies on gas storage capacity of marine and continental shales in the Sichuan Basin, China," *Journal of Natural Gas Science and Engineering*, vol. 36, pp. 773–785, 2016.

[47] H. Shi, L. Song, H. Zhang et al., "Experimental and numerical studies on progressive debonding of grouted rock bolts," *Mining Science and Technology*, vol. 32, no. 1, pp. 63–74, 2022.

[48] Y. Xue, P. G. Ranjith, F. Gao, Z. Zhang, and S. Wang, "Experimental investigations on effects of gas pressure on mechanical behaviors and failure characteristic of coals," *Journal of Rock Mechanics and Geotechnical Engineering*, vol. 15, no. 2, pp. 412–428, 2023.

[49] Y. Zhang, Y. Wu, Y. Teng, P. Li, and S. H. Peng, "Experiment study on the evolution of permeability and heat recovery efficiency in fractured granite with proppants," *Geomechanics and Geophysics for Geo-Energy and Geo-Resources*, vol. 8, no. 1, 2022.

[50] Y. Wu, P. Li, Y. Hao, A. Wanniarachchi, Y. Zhang, and S. H. Peng, "Experimental research on carbon storage in a CO_2-based enhanced geothermal system," *Renewable Energy*, vol. 175, pp. 68–79, 2021.

[51] A. R. Biedermann, C. B. Koch, W. Lorenz, and A. M. Hirt, "Low-temperature magnetic anisotropy in micas and chlorite," *Tectonophysics*, vol. 629, pp. 63–74, 2014.

[52] Y. Cao, J. Du, M. Park et al., "Metastability and nondislocation-based deformation mechanisms of the flem eclogite in the Western Gneiss Region, Norway," *Journal of Geophysical Research - Solid Earth*, vol. 125, no. 5, 2020.

[53] Z. T. Lv, C. C. Xia, Y. S. Wang, and Z. L. Lin, "Frost heave and freezing processes of saturated rock with an open crack under different freezing conditions," *Frontiers of Structural and Civil Engineering*, vol. 14, no. 4, pp. 947–960, 2020.

[54] G. W. Scherer, "Crystallization in pores," *Cement and Concrete Research*, vol. 29, no. 8, pp. 1347–1358, 1999.

[55] S. Peppin and R. W. Style, "The physics of frost heave and ice-lens growth," *Vadose Zone Journal*, vol. 12, no. 1, article vzj2012.0049, 2012.

[56] L. J. Van Alst, "Laboratory experiments in cold temperature rock deformation, [Ph.D. thesis]," University of Oregon, 2011.